International Journal of Low-Carbon Technologies, 2025, **20**, 1627–1637
https://doi.org/10.1093/ijlct/ctaf094
Original Article

High-fidelity numerical analysis of the interaction between the unsteady flow and the blade structure oscillation of a marine current turbine

Shine Win Naung[1,*], Yufeng Yao[1], Ceri Morris[1], Allan Mason-Jones[2], Amir Keshmiri[3]

[1]School of Engineering, The University of the West of England, Frenchay Campus, Coldharbour Lane, Bristol BS16 1QY, United Kingdom
[2]School of Engineering, Cardiff University, Queen's Buildings, The Parade, Cardiff CF24 3AA , United Kingdom
[3]School of Engineering, The University of Manchester, The Engineering Building A, Booth Street E, Manchester M13 9QS, United Kingdom

*Corresponding author. School of Engineering, The University of the West of England, Frenchay Campus, Coldharbour Lane, Bristol BS16 1QY, UK.
E-mail: Shine.WinNaung@uwe.ac.uk

Abstract

Marine current energy is a promising renewable resource due to its predictability. However, marine current turbines face unsteady loading, which can influence the turbine performance. This study models the interaction between the unsteady flow and blade oscillation using a coupled computational fluid dynamics–finite element analysis method. A nonlinear frequency domain solution method is proposed and extensively validated. Results show that blade oscillation impacts the hydrodynamic and hydroelastic performance of the blade and increases thrust, torque, and power coefficients by 5.5 times compared to a rigid blade case. The frequency domain solution method accurately predicts performance while reducing the computation time to only 2.5 hours.

Keywords: marine current turbines; hydrodynamics; hydroelasticity; fluid–structure interaction; computational fluid dynamics

Nomenclature

Latin Letters	
A_U	Fourier coefficient for the conservative variables
B_U	Fourier coefficient for the conservative variables
$[C]$	Damping matrix
C_p	Time-averaged pressure coefficient
C_{p1}	Unsteady pressure amplitude coefficient
D	Rotor diameter [m]
$\vec{d}$	Displacement [m]
$\vec{f}$	External force [N]
$\vec{F}_I$	Inviscid flux term
$\vec{F}_V$	Viscous flux term
$[K]$	Stiffness matrix
$[M]$	Mass matrix
m	Number of harmonics
n_{modes}	Number of selected modes
P	Unsteady pressure [Pa]
$\overline{P}$	Time-averaged pressure [Pa]
P_A	Fourier coefficient for the unsteady pressure
P_{Amp}	Amplitude of the unsteady pressure [Pa]
P_B	Fourier coefficient for the unsteady pressure
$\overline{q}$	Mean generalised displacement
q_A	Amplitude of the generalised displacement
q_i	Generalized displacement
R	Rotor radius [m]
R_L	Lumped residuals and source terms
S	Surface [m^2]
S_T	Source term
t	Time [s]
U	Conservative flow variables
$\overline{U}$	Time-averaged flow variables

Greek Letters	
ξ_i	Damping coefficient
$\vec{\phi}_i$	Mode shape
Ω	Control volume [m^3]
ω	Fundamental frequency [rad/s]
ω_i	Natural frequency for the i mode [rad/s]

1 Introduction

Over the past 20 years, interest in the design and performance of horizontal-axis hydrokinetic tidal turbines has increased. Progress in the latter field has evolved from small-scale laboratory experiments in the early 2000s to full-scale devices as of 2024 [1]. However, challenges persist, especially in relation to structural design, life expectancy, and subsequent maintenance. Moreover, the technology has not yet achieved cost-effectiveness compared to other renewable sources such as offshore wind. It has also been estimated that tidal stream energy's levelized cost of energy (LCOE) will be £259 ± 30/MWh, with the potential for a reduction to £193 ± 48/MWh by 2026. Further projections suggest that between 2030 and 2035, the LCOE for tidal stream is expected to further decrease to £116 ± 38 and £78 ± 25/MWh, respectively. These estimates are contingent on the cumulative tidal stream turbine deployment of 877 MW in the UK and 783 MW in France by 2035. This represents a substantial increase in available power over the next 11 years, starting from 2024, and will require

Received 11 November 2024; revised 11 April 2025; accepted 16 June 2025

strong commitments from governments, stakeholders, and industries [2]. A key focus is to reduce the cost of energy generation and the reliability of device performance. Therefore, there is a requirement to continue research into turbine performance and the continued improvement of associated experimental and numerical methods, such as computational fluid dynamics (CFD). CFD models can be used for the evaluation of energy extraction performance, loads, wake effects, and wave interactions. However, challenges exist due to high computational expense, which opens up the possibility to employ other modelling techniques to model blade hydrodynamic performance and kinetic energy extraction.

The blade element momentum (BEM) method is widely utilised in designing marine current turbines due to its advantages of rapid computation and the ability to produce reasonable results with available aerofoil data [3]. However, BEM models have various limitations and require empirical corrections to enhance their accuracy [4]. Despite these corrections, BEM models cannot provide detailed flow information, resulting in an incomplete understanding of the unsteady flow physics around turbines. For wake analysis of tidal turbines, vortex models and actuator-type models have been developed [5, 6]. Most vortex models either ignore viscous effects or need complex modifications to include them, while actuator-type models, which represent rotors or blades as disks or lines without the real geometry, are typically used in combination with fluid flow solvers such as CFD solvers [7]. Similar to BEM models, actuator-type models rely on aerofoil data for calculating blade loading and are more time-consuming and computationally intensive than BEM models. CFD methods are considered great alternatives to experiments as they can capture detailed flow information depending on the accuracy of turbulence modelling. Unsteady Reynolds-averaged Navier–Stokes (URANS) models, which utilise a turbulence model to simulate turbulent flow, are commonly employed for the modelling and simulations of marine current turbines [8, 9].

CFD methods are typically coupled with finite element analysis (FEA) methods to model fluid–structure interaction (FSI). There are different coupling strategies, traditionally known as one-way coupling or two-way coupling approaches, depending on the desired accuracy and available computational resources. Wang *et al.* [10] used a one-way coupling method, which coupled CFD and FEA models, to investigate the deformation and stress distribution of a blade by applying the fluid pressure, extracted from the CFD simulation, on the blade. Jiao *et al.* [11] employed a fully coupled CFD and FEA method to analyse the hydroelastic responses of a marine structure. Yang *et al.* [12] also proposed an advanced fully coupled FSI model, coupling a URANS model and a finite element model, to predict the structural responses and performance of a vertical-axis tidal turbine operating in complex and turbulent flow conditions. A high-fidelity CFD model was coupled with an FEA model in a numerical study of Win Naung *et al.* [13] to thoroughly investigate the impact of the structural deformation and oscillation on the unsteady flow behaviour of a marine propeller. It was found that the coupled CFD–FEA models were highly effective in modelling and analysing the complex interaction between the fluid flow and elastic structures. In these studies, the flow-governing equations are solved in the time domain, referred to as time domain methods in this study. The main drawback of traditional time domain methods is that they are computationally expensive and often not feasible for industrial applications.

Frequency domain methods including a harmonic balance method, developed by Hall *et al.* [14] and He [15], have become very popular for turbomachinery analysis due to their computational efficiency and reasonable accuracy. Rahmati *et al.* [16] introduced a nonlinear frequency domain solution approach for analysing the aeroelasticity of turbomachines, including compressors, gas turbines, and low-pressure turbines. Their research demonstrated that a fully integrated turbine model provides more accurate predictions of the unsteady flow behaviour encountered in a turbomachine compared to a simplified model such as an isolated blade model [17]. Recently, frequency domain methods have been extended to the aerodynamic and aeroelastic analysis of wind turbines [18, 19]. They used a nonlinear frequency domain solution method to evaluate the impacts of inflow turbulence and wake on the aerodynamic and aeromechanical performance of a wind turbine. Their work was further expanded to include an aerodynamic analysis of wind turbines in an array with a tower, using the nonlinear frequency domain solution method [20]. It was highlighted that the frequency domain methods could reduce the computational cost by one to two orders of magnitude, compared to conventional time domain solution methods, without compromising the required accuracy. While the frequency domain methods have been widely used for turbomachinery analysis including wind turbines, it is relatively new for the analysis of marine current turbines.

This study applies the frequency domain solution method to characterise the performance of a three-bladed horizontal-axis tidal turbine. The results obtained are compared with those from a previously validated CFD model [21–23] as well as a traditional time domain solution method. Additionally, the method is used to investigate blade oscillation and its influence on the hydrodynamic and hydroelastic performance of the blade, including unsteady pressure distribution, hydrodynamic loads and damping while highlighting the computational efficiency and accuracy for the modelling and analysis of the hydroelastic behaviour of marine current turbines.

2 Methodology

This study employs a CFD method and an FEA method to model the interaction between the fluid flow and the marine current turbine rotor. In particular, this paper uses a nonlinear frequency domain solution method, as described in Ref. [18], to solve the flow-governing equations and to model the hydroelasticity of the marine current turbine.

2.1. CFD modelling

The flow is governed by the Navier–Stokes equations, which, in a Cartesian coordinate system, can be written as [18]:

$$\frac{\partial}{\partial t}\int_{\Omega} U\mathrm{d}\Omega + \int_{S} \overrightarrow{F}_I.\mathrm{d}\overrightarrow{S} + \int_{S} \overrightarrow{F}_V.\mathrm{d}\overrightarrow{S} = \int_{\Omega} S_T\mathrm{d}\Omega \quad (1)$$

In this equation, Ω represents the volume, S denotes the surface, U denotes the conservative variables, S_T represents the source term, and $\overrightarrow{F}_V$ and $\overrightarrow{F}_I$ are the viscous and inviscid fluxes, respectively. This study employs a URANS model, utilising the k-ω SST model for turbulence modelling. Governing equation (1) can be expressed in a semidiscrete form as

follows:

$$\frac{\partial}{\partial t}(U) = R_L \tag{2}$$

In this equation, R_L represents both the lumped residuals and the source terms.

Typically, the URANS equations are solved at each time step, and this approach is termed the time domain solution method, as explained in Ref. [16], in this paper. Using the proposed frequency domain solution method, the conservative flow variables U can be separated into the mean component and unsteady fluctuations over periodic cycles. It can, therefore, be described using a Fourier series, defined by a fundamental frequency, ω, which corresponds to the blade passing frequency or the blade vibration frequency, and a specified number of harmonics, m, as shown in equation (3). In this paper, both the time domain solution method and the frequency domain solution method are used and compared to each other.

$$U = \overline{U} + \sum_{m=1}^{M} [A_U \sin(m\omega t) + B_U \cos(m\omega t)] \tag{3}$$

where $\overline{U}$, A_U, and B_U represent the Fourier coefficients, M is the maximum number of harmonics, and t is the time. The order of the Fourier series or the number of harmonics can be tuned to control the accuracy of the flow solution. Substituting equation (3) into equation (2) results in a new set of unsteady Navier–Stokes equations, as expressed in equation (4).

$$\omega \sum_{m=1}^{M} [mA_U \cos(m\omega t) - mB_U \sin(m\omega t)] = R_L \tag{4}$$

Using the frequency domain solution method, employed in this paper, the modified set of Navier–Stokes equations (i.e. equation (4)) is solved in the frequency domain. The unsteady period is then divided into $N = (2\,m + 1)$ time levels, and the system of nonlinear equations is solved iteratively. The detailed formulation of the nonlinear frequency domain solution method can be found in Refs. [18, 19]. Fundamental mode or one harmonic (i.e. $m = 1$) is considered sufficient for the modelling discussed in this paper. Using one harmonic, equations (3) and (4) can be rewritten as:

$$U = \overline{U} + [\,A_U \sin(\omega t) + B_U \cos(\omega t)] \tag{5}$$

$$\omega\,[A_U \cos(\omega t) - B_U \sin(\omega t)] = R_L \tag{6}$$

Equation (6) can be expressed at three temporal phases as follows.

$$U_0 = \overline{U} + B_U \qquad At\ \omega t = 0 \tag{7.1}$$

$$U_{\pi/2} = \overline{U} + A_U \qquad At\ \omega t = \pi/2 \tag{7.2}$$

$$U_{-\pi/2} = \overline{U} - A_U \qquad At\ \omega t = -\pi/2 \tag{7.3}$$

The three Fourier coefficients can be determined using the above three equations. Equations (8.1)–(8.3) are written by substituting these coefficients into equation (6).

$$\omega\left(\frac{U_{\pi/2} - U_{-\pi/2}}{2}\right) - R_{L0} = 0 \tag{8.1}$$

$$\omega\left(U_0 - \frac{U_{\pi/2} + U_{-\pi/2}}{2}\right) + R_{L\pi/2} = 0 \tag{8.2}$$

$$\omega\left(U_0 - \frac{U_{\pi/2} + U_{-\pi/2}}{2}\right) - R_{L-\pi/2} = 0 \tag{8.3}$$

The new sets of Navier–Stokes equations are simultaneously solved by a CFD solver in a similar way to that of the steady-state equations with the extra term being treated as a source term. The detailed mathematical formulation of the frequency domain solution can be found in Refs. [16, 18]. A second-order upwind scheme is used for the spatial discretisation, and a second-order Backward Euler method is used for the temporal discretisation with the time domain method, as discussed in Ref. [24]. The residual targets are set to 10^{-6} for both time domain and frequency domain solutions to ensure that the solution is fully converged.

2.2. Structural modelling

An FEA method is used for the modelling of the structural deformation. The solid mechanics is governed by equation (9).

$$[M]\frac{\partial^2 \vec{d}}{\partial t^2} + [C]\frac{\partial \vec{d}}{\partial t} + [K]\vec{d} = \vec{f} \tag{9}$$

In this equation, $\vec{d}$ denotes the displacement, $\vec{f}$ denotes the external force including hydrodynamic force, gravitational force, and centrifugal force, and $[M]$, $[C]$, and $[K]$ represent the mass matrix, the damping matrix, and the stiffness matrix, respectively.

The overall displacement of the blade structure can be expressed as:

$$\vec{d} = \sum_{i=1}^{n_{modes}} q_i \vec{\phi}_i \tag{10}$$

where q_i represents the generalised displacement, $\vec{\phi}_i$ represents the mode shape of the blade structure normalised by the mass, and n_{modes} denotes the number of selected modes. By applying equation (10) in the modal equation, assuming Rayleigh damping and selecting an appropriate scale factor for the mode shape, a set of independent equations for each mode can be derived as shown in equation (11).

$$\frac{d^2 q_i}{dt^2} + 2\xi_i \omega_i \frac{dq_i}{dt} + \omega_i^2 q_i = \vec{\phi}_i^{\,T} \vec{f} \tag{11}$$

where ξ_i is the damping coefficient for each mode shape and ω_i is the natural frequency. The generalised displacement q_i must be defined for the desired oscillation amplitude and can be expressed as:

$$q_i(t) = \overline{q} + q_A \sin(\omega_i t) \tag{12}$$

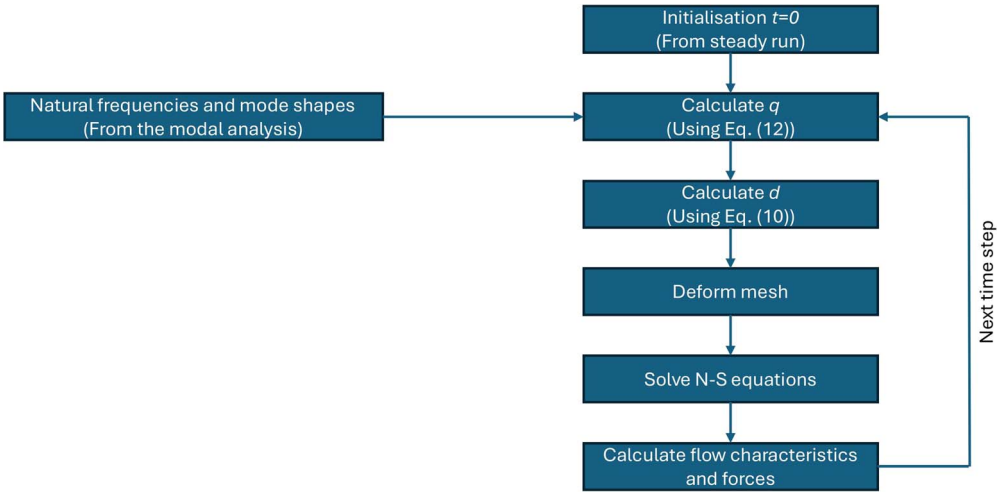

Figure 1. Flow chart of the FSI modelling.

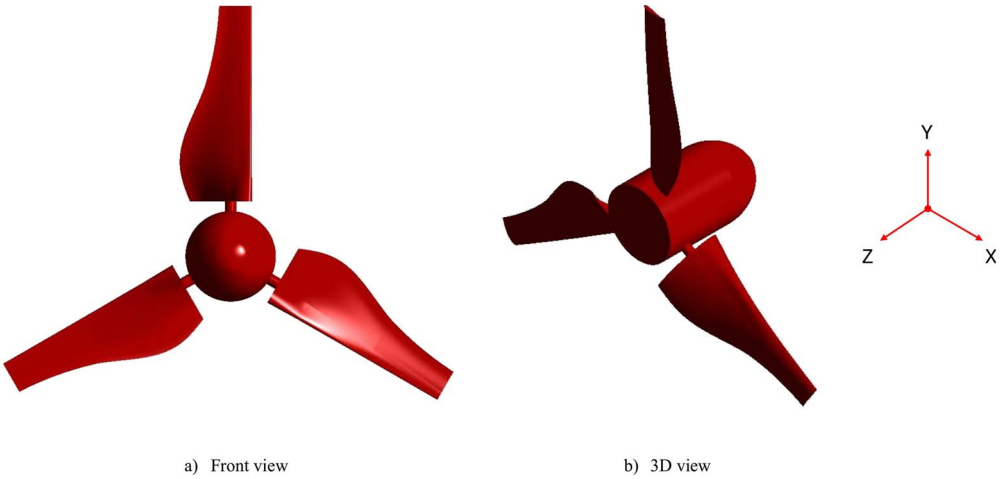

Figure 2. Geometry of the employed marine current turbine rotor (diameter = 10 m).

In this equation, $\overline{q}$ is the mean value of the blade displacement and q_A is the amplitude of the blade oscillation. With this information, the CFD solver computes the overall blade deformation and subsequently solves the flow-governing equations using the deformed blade. The detailed formulation of the structural modelling can be seen in Refs. [18, 19]. The structural steel is used as the material of the blade, which possesses a density of 7850 kg/m^3, a Young's modulus of 2×10^{11} Pa, and a Poisson's ratio of 0.3, to be similar to the material of the scaled turbine model used for the experimental testing in [23].

2.3. Modelling of FSI

An overview of the detailed solution procedure is provided in this section. A modal coupling method is employed for the FSI modelling. A crucial preprocessing step prior to the CFD modelling involves a modal analysis using an FEA method to calculate the natural frequencies and the mode shapes of the blade structure. A steady-state CFD simulation is initially conducted to set as an initial condition for the unsteady computation. The selected frequency and the mode shape (i.e. first vibration mode) are then imported into the CFD solver as a mode shape profile ($\vec{\phi}_i$ in equation (10)) to facilitate the blade structural oscillation in the flow computation. The frequency and the generalised displacement in equation (12) need to be specified to obtain the desired oscillation frequency and amplitude, which is used to compute the deformation of the blade in equation (10). Based on the specified generalised displacement, the flow solver determines the total blade deformation and accordingly updates the fluid mesh to conform to the moving blade boundary using a displacement diffusion method [25]. Using the updated mesh, an unsteady CFD simulation is carried out using both the time domain and frequency domain solution methods. In the time domain solution procedure, the unsteady CFD solver directly simulates the transient fluid flow in response to the oscillating blade by stepping through discrete time intervals and calculating the evolving hydrodynamic loads on the blade at each time step. A significant reduction in computation time can be achieved using the frequency domain solution method, which, unlike the time domain solution, does not require solving the solution in time over many oscillation cycles to reach a steady-periodic state. The solution computed by the frequency domain method can be reconstructed in time to obtain a time history of the flow solution, as discussed in Ref. [16, 18]. The flow chart of the FSI modelling is presented in Fig. 1.

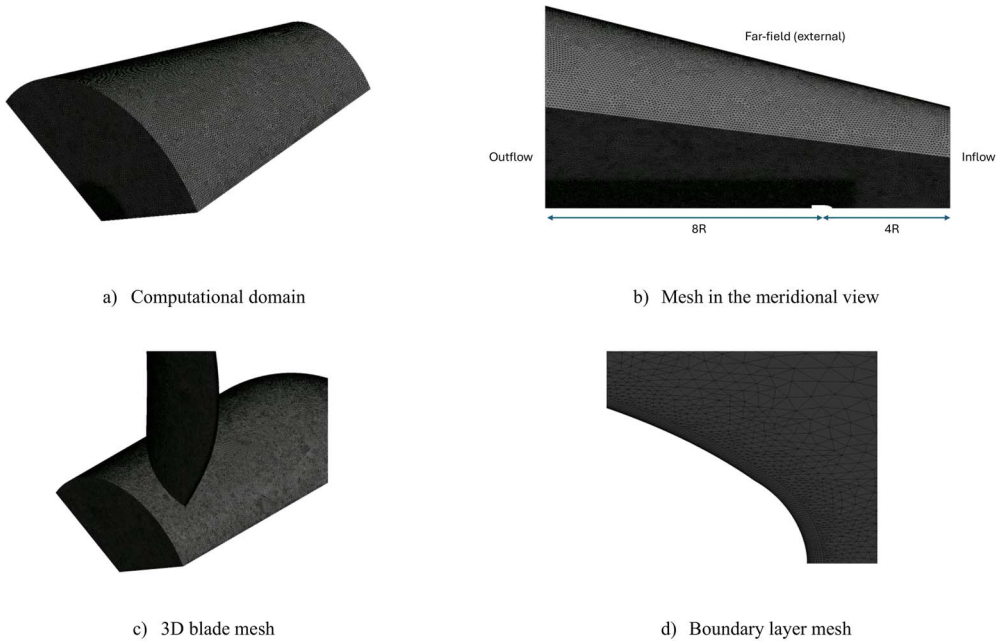

Figure 3. Computational domain and mesh of the marine current turbine rotor.

2.4. Computational domain and mesh

The work presented in this paper is based on a three-bladed horizontal-axis marine current turbine rotor, utilising a Wortmann FX 63-137 profile with a 33° twist from the root to the tip, as described in Ref. [22]. The details of the geometry, experimental validations, and the nondimensional scaling of different rotor diameters are extensively discussed in Ref. [23]. The 10-m diameter rotor model is employed for the present paper. The geometry of the rotor model can be seen in Fig. 2. A Cartesian coordinate system is employed to construct the model. The frontal area of the turbine lies on the X–Y plane, and the rotor rotates along the Z-axis.

Figure 3 illustrates the generated computational domain and mesh. Only one-third of the rotor is modelled in this analysis to reduce the total computational cost, with the use of periodic boundaries. The domain has a conical shape, with the outlet radius being twice the size of the inlet radius to account for the wake expansion in the downstream region. The inlet and outlet are located 4R upstream and 8R downstream of the rotor, respectively, where R is the rotor radius. An unstructured mesh is used to generate the mesh employed in this analysis. The mesh around the rotor and the wake region are locally refined to resolve the wake structures and the unsteady flow behaviour (Fig. 3). The boundary layer mesh is created using 20 layers with a growth rate of 1.2. The first-layer thickness is carefully selected to ensure the y^+ value is less than unity. There are 15.8×10^6 elements in the single passage domain, which is considered adequate to accurately resolve the necessary flow details for the present work. The mesh employed in this study features a higher resolution than that of the previously validated study by Morris *et al.* [22] and is similar to that of the high-fidelity study by Win Naung *et al.* [13].

2.5. Boundary conditions

A uniform freestream inflow velocity of 3.086 m/s is applied at the inlet and far-field (external) boundaries. The rotational speed of the rotor is varied to achieve the desired tip speed ratio (TSR). The peak power is achieved at the TSR of 3.6, which results in the rotational speed of 2.25 rad/s. A TSR of 3.6 is selected for the unsteady simulations involving the blade structural oscillation. A no-slip wall boundary condition is applied to the blade and the hub surfaces. A pressure-outlet boundary is defined at the outlet. A rotating frame of reference is implemented to model the rotation of the rotor.

3 Results and discussions

3.1. Validation

Before performing the hydroelastic simulations integrating the blade oscillation, the steady-state simulations for a rigid blade for various TSRs are conducted and compared to the results of Morris *et al.* [22], which has also been validated against the experiment of Mason-Jones *et al.* [23]. The validations are performed in terms of the power coefficient and the torque coefficient. Figure 4 demonstrates the comparisons of the power and torque coefficients obtained from the present simulations with that of Ref. [22]. It is seen that the results from both studies are close to each other with minor discrepancies within 6%.

3.2. Hydroelastic analysis of the marine current turbine rotor blade

After the CFD model has been validated for various TSRs against the reference study, hydroelastic simulations are carried out to investigate the interaction between the unsteady flow and the blade structure oscillation. The modal coupling method is employed for the modelling of FSI in this analysis, as described in Section 2. The modal analysis is initially performed to determine the natural frequencies and the mode shape of the marine current turbine blade. As discussed in Section 2, the first vibration mode is used for the hydroelastic analysis. As in the aeromechanical analyses discussed in Ref. [17], the first natural frequency is defined as the vibration frequency in this paper (i.e. 11.484 Hz). The mode shape of the blade associated with the first natural frequency is shown

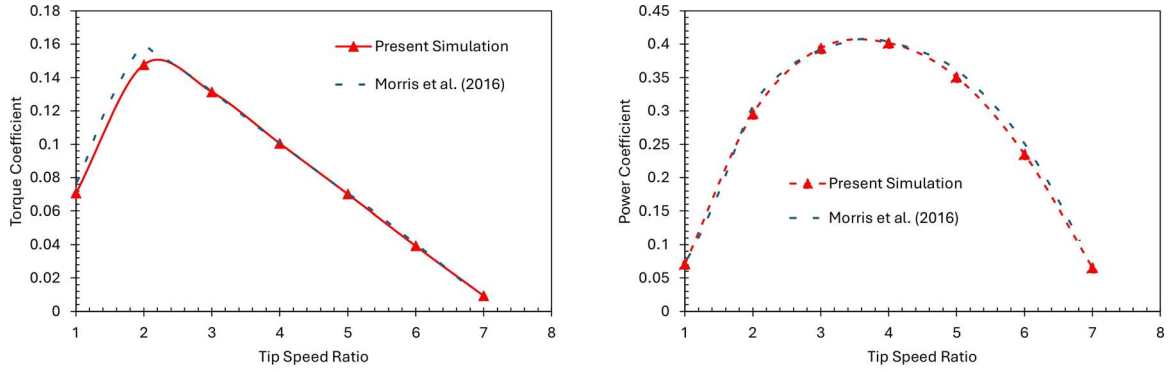

a) Torque Coefficient b) Power Coefficient

Figure 4. Comparisons of torque and power coefficients between the present work and that of Ref. [22].

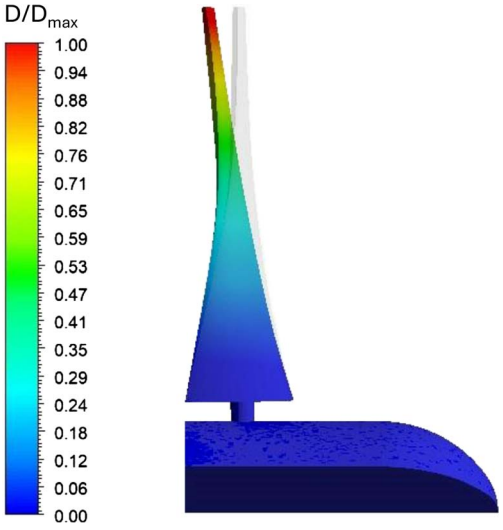

Figure 5. The first vibration mode of the marine current turbine blade.

in Fig. 5. It is presented as the dimensionless displacement contour, and the undeformed shape of the blade is also added to better visualise the vibration mode. In the hydroelastic simulations, the maximum amplitude of oscillation is set to the desired 2% of the blade span as the marine current turbines are typically rigid and the oscillation amplitudes can be relatively small. A preliminary one-way coupling FSI analysis (not shown in this paper) suggested that the 2% span deflection is deemed appropriate.

The hydroelastic simulations are primarily conducted using the nonlinear frequency domain solution method. As no experimental or numerical results are available for this analysis, the results are compared to the traditional time domain solution CFD method, which is performed in addition to the frequency domain solution, for validation. The pressure distribution over the marine current turbine blade can be decomposed into the time-averaged component and the unsteady fluctuation, as expressed in equation (13).

$$P = \overline{P} + P_A \sin(\omega t) + P_B \cos(\omega t) \tag{13}$$

In this equation, $\overline{P}$ is the mean pressure, and P_A and P_B are the Fourier coefficients. The unsteady pressure amplitude (P_{Amp}) can be expressed as [19]:

$$P_{Amp} = \sqrt{{P_A}^2 + {P_B}^2} \tag{14}$$

The unsteady pressure distribution over a blade surface is typically presented as the time-averaged pressure coefficient, denoted as C_p, and the unsteady pressure amplitude coefficient, C_{p1}. Both the time-averaged pressure and the unsteady pressure amplitude are normalised by the dynamic pressure to calculate the coefficients C_p and C_{p1}. The comparisons of C_p between the rigid blade case and the oscillating blade case at the 30% span and 90% span blade sections, obtained from the frequency domain solution method, are demonstrated in Fig. 6. It is observed that there is only a slight deviation between the two cases at 30% span section. This is expected as this is close to the hub and the blade oscillation is relatively small in this region. At the 50% span section (not shown), the difference becomes noticeable. Greater deviations between the two cases are detected at the 70% span and 90% span sections due to large oscillation amplitudes. Figure 7 presents the comparison of C_{p1} between the frequency domain solution method and the time domain solution method at the 30% span and 90% span blade sections. As seen, both the frequency domain and time domain methods agree well with each other, which indicates that the frequency domain solution method accurately predicted the unsteady pressure distribution over the blade surfaces. Strong agreements between the time domain and frequency domain methods are also observed for both C_p and C_{p1} at different blade sections, but they are now shown to make the paper concise as the results are very similar. The effect of the blade oscillation is more pronounced in the outer region, with nearly 13% difference in the area-averaged pressure distribution between the two cases along the aerofoil chord at the 90% blade span section compared to 0.5% at the 30% span section, as the amplitude of the oscillation is larger in the blade tip regions due to the first bending mode being considered. This is also in agreement with the unsteady pressure distribution seen in Fig. 6. Results clearly indicate that the oscillation has a great impact on the hydrodynamic performance of the turbine, influencing the pressure distribution over the surfaces.

The comparisons of the thrust, torque, and power coefficients between the rigid and oscillating blade cases over two oscillation cycles are illustrated in Fig. 8. These data are extracted after the flow achieves a steady and periodic

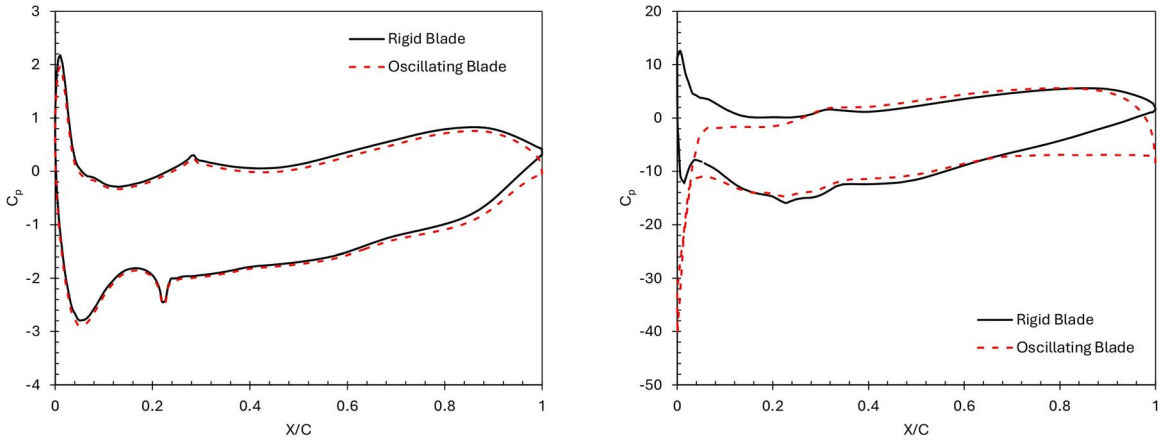

a) C_p at 30% Span b) C_p at 90% Span

Figure 6. Comparisons of C_p between the rigid blade case and the oscillating blade case.

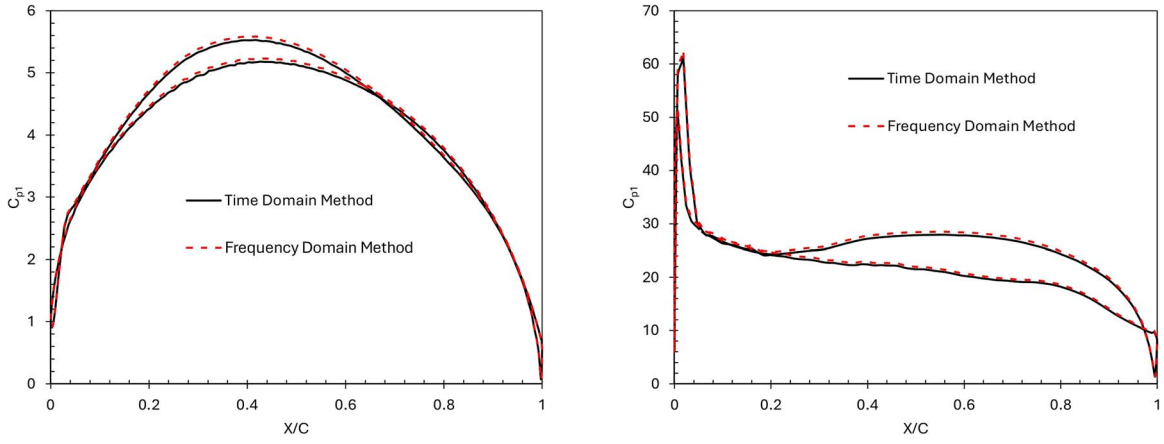

a) C_{p1} at 30% Span b) C_{p1} at 90% Span

Figure 7. Comparisons of C_{p1} between the time domain solution method and the frequency domain solution method.

state after 10 cycles of oscillation. For the oscillating blade case, both the time domain and frequency domain solution methods are utilised to compute these coefficients, showing close agreement. The periodic motion of the blade results in a sine wave force distribution over the oscillation cycle, in contrast to the steady force coefficient observed for the rigid blade. This indicates that the oscillating blade introduces a dynamic force component, characterised by the frequency and amplitude of the blade structural oscillation. Notably, an oscillation amplitude of 2% span results in a cyclic variation of hydrodynamic loads with the peak amplitude of coefficients being approximately 5.5 times greater than that of the rigid blade. Close agreement between the time and frequency domain methods validates the accuracy of the frequency domain solution method for the calculation of hydrodynamic loads applied on the oscillating blade.

The stability of the oscillating blade can be determined by the hydrodynamic damping ratio, which is the ratio of the hydrodynamic work per oscillation cycle to the kinetic energy of the blade. The oscillation of the blade structure can be considered stable if the hydrodynamic damping ratio is positive. In this study, the hydrodynamic damping ratio is calculated by both the time domain solution method and the frequency domain solution method, as presented in Table 1.

Table 1. Hydrodynamic damping ratio computed by the time domain and frequency domain methods

Method	Hydrodynamic damping ratio
Time domain solution method	0.07
Frequency domain solution method	0.06

Both results are in close agreement and show that the hydrodynamic damping ratio is positive, which indicates that the blade oscillation is stable in the present study.

The velocity contours between the rigid blade and oscillating blade cases, as shown in Fig. 9, reveal distinct differences in the rotor region. While the overall flow field appears similar in both scenarios, it highlights that the oscillating blade induces a significantly stronger velocity field around the rotor. This behaviour is attributed to the periodic motion of the blade, which introduces dynamic effects to the velocity field. The oscillation of the blade introduces periodic flow disturbances, which continuously disrupt the flow around the blade. These effects lead to enhancing vortex generation and the local velocity magnitudes in the flow field, close to the blade surfaces, potentially impacting rotor performance and

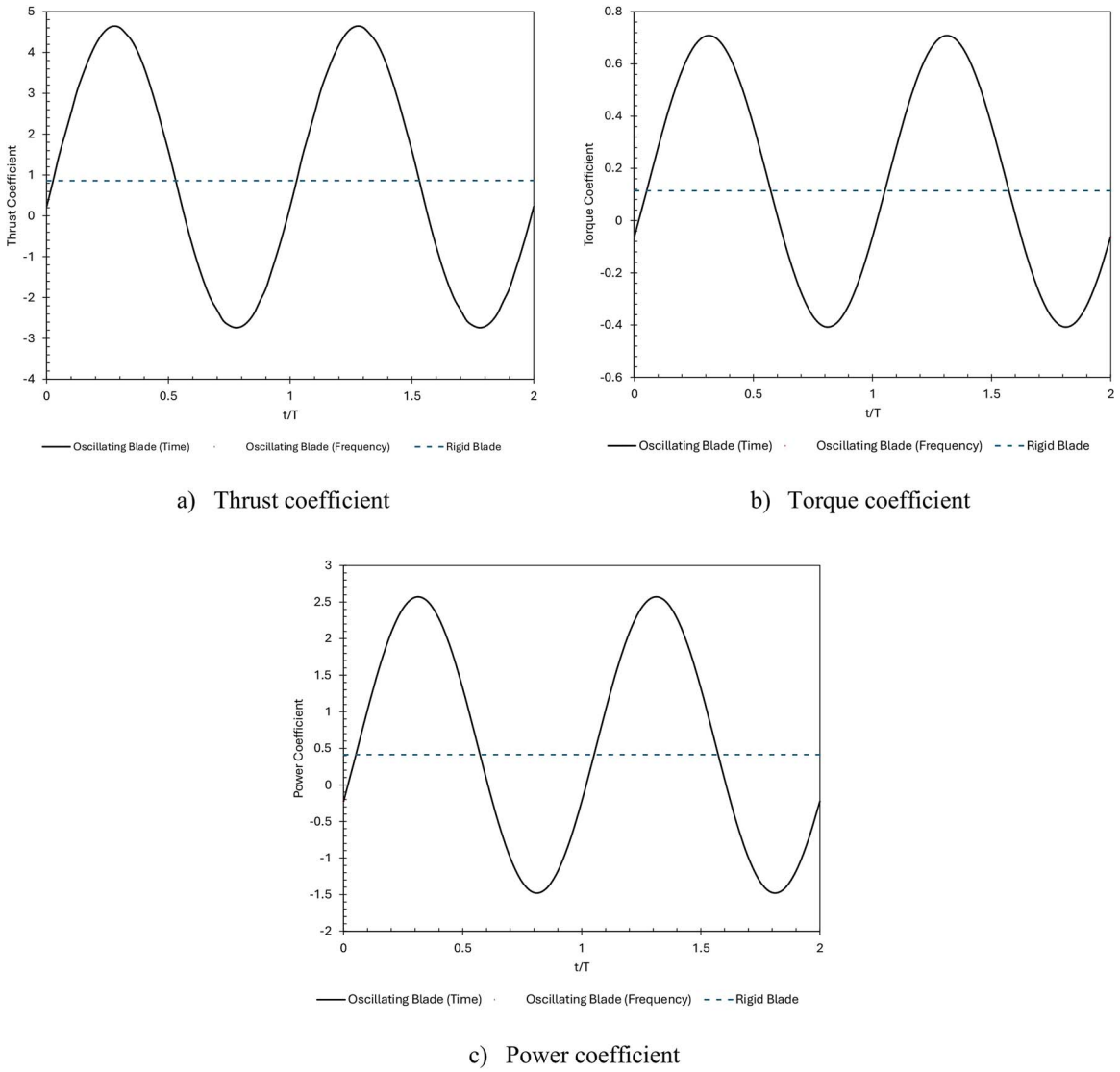

Figure 8. Variations of thrust, torque, and power coefficients over two oscillation cycles.

efficiency of the turbine (Fig. 9b). This observation indicates the importance of considering the hydroelastic behaviour of the marine current turbines and their influence on the overall performance. The effects of the blade oscillation on the flow can be better visualised using the flow streamlines and isosurface. Figure 10 illustrates velocity streamlines and vorticity isosurface, coloured by velocity for the oscillating blade case. The streamlines are equally spaced, originating from the blade. The oscillating blade produces noticeably stronger streamlines, attributed to its periodic motion, which introduces additional disturbances to the surrounding fluid. Moreover, the oscillating motion of the blade induces greater mixing of the streamlines in the wake region. Figure 10b shows the isosurface of the vorticity, initiated from the blade within the initial oscillation period, which shows flow disturbances to the tip vorticity generation due to the periodic oscillation of the blade.

Figure 11 presents the analyses of wake profiles or velocity profiles, normalised by the reference velocity, in the downstream region of the turbine. The profiles are extracted at different downstream locations such as Z = 0.5D, 1D, 2D, and 3D, where D is the rotor diameter, on a horizontal plane, parallel to the rotation axis (i.e. Z–X plane as shown in Fig. 2), at 90% blade span. At the 0.5D distance, the wake profiles are compared between the rigid and oscillating blade cases. It is evident that blade oscillation introduces a slight distortion to the wake, influencing the shape and behaviour of the wake profile. However, since it depends on the frequency and amplitude of the structural oscillation, further investigations are required to thoroughly investigate the effects of the blade vibration on the wake profiles by considering different frequencies and amplitudes of the oscillation. Figure 11b further shows the wake recovery process at different downstream positions. It is seen that the wake remains strongly influenced by the rotor at the 3D distance as expected.

Figure 12 illustrates the wall work density distribution over the marine current turbine blade, highlighting distinct stabilisation and destabilisation effects on different sides of the blade. The pressure side of the blade exhibits a dominant stabilisation effect, effectively maintaining the stability of the blade. Conversely, the suction side shows a mixed destabilisation effect, indicating varying degrees of instability. This combination of these effects results in a positive

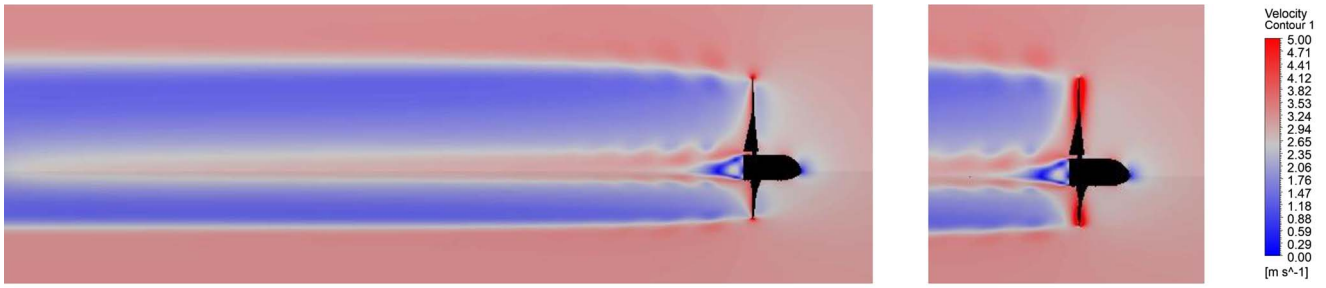

a) Velocity field in the rigid blade case b) Velocity field around the oscillating blade

Figure 9. Velocity field in the meridional view obtained from the rigid and oscillating blade cases obtained from the frequency domain solution.

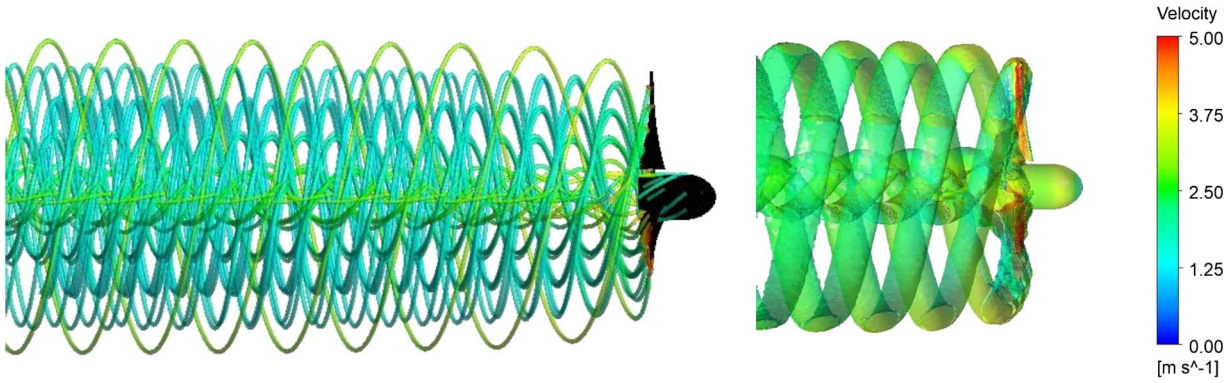

a) Flow streamlines b) Vorticity iso-surfaces

Figure 10. Velocity streamlines and vorticity isosurface generated from the oscillating blade obtained from the frequency domain solution.

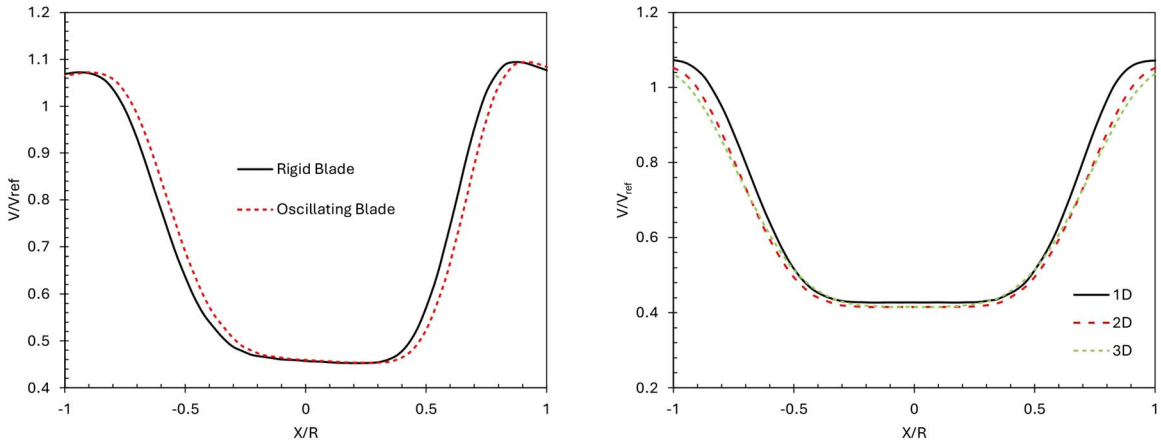

a) Wake profile at 0.5D b) Wake profile at 1D, 2D and 3D

Figure 11. (a) Comparison of wake profiles at 0.5D between the rigid blade case and the oscillating blade case, and (b) comparison of wake profiles at different downstream locations from the oscillating blade case (profiles extracted on the Z–X plane at Y = 90% span).

hydrodynamic damping, as seen in Table 1, which is beneficial for the performance of the turbine. Positive hydrodynamic damping contributes to the stability and efficiency of the turbine by reducing oscillations of the blade structure.

The simulations presented in this paper are conducted on a high-performance computing cluster using 96 cores. The total computational costs registered by the time domain solution method and the frequency domain solution method are listed in Table 2. The table reveals that the frequency domain method can save a significant amount of computation time, compared to the time domain method, without compromising the required accuracy and flow resolution.

4 Conclusions

In this paper, the interaction between the unsteady flow and the blade structure oscillation of a marine current turbine was investigated using CFD simulations. In particular, the nonlinear frequency domain solution method was applied to the FSI

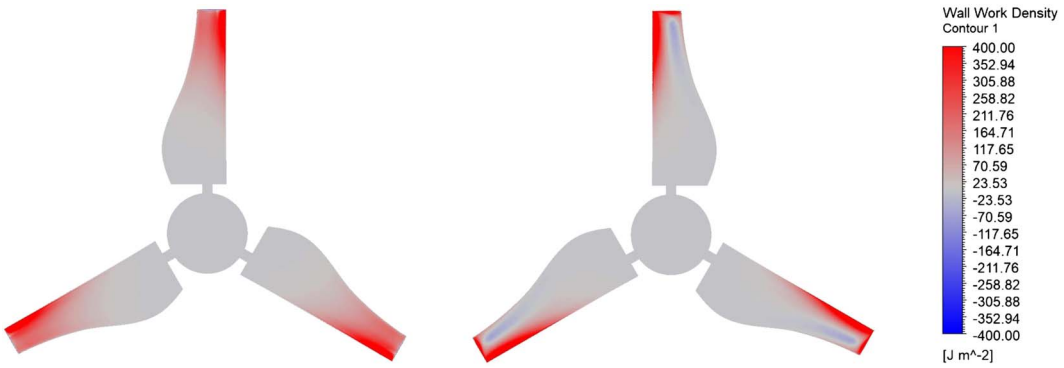

a) Pressure side b) Suction side

Figure 12. Wall work density contours over the pressure and suction surfaces of the oscillating blade.

Table 2. Computational costs required by the time domain and frequency domain methods

Method	Computation time (hours)
Time domain solution method	60
Frequency domain solution method	2.5

modelling of the blade. The employed CFD model was initially validated against the reference study, and a close agreement with minor discrepancies within 6% was obtained between the present work and the reference study. The first natural frequency (11.484 Hz), obtained from the modal analysis, is defined as the oscillation frequency with an amplitude of 2% blade span in the hydroelastic simulation. The analysis revealed that the hydroelastic performance of the blade was primarily affected by the blade structural oscillation. Due to the characteristics of the bending mode, the tip region of the blade was more influenced by the oscillation as a notable difference in the pressure distribution (13% difference at the 90% span section compared to 0.5% at the 30% span) was detected between the oscillating blade case and the rigid blade case. The dynamic motion of the blade resulted in a periodic variation of hydrodynamic load and power distributions over the blade, with the peak amplitude being approximately 5.5 times higher than that of the rigid blade. The hydrodynamic damping of the blade was utilised to determine the stability of the blade, which indicated that the blade oscillation was considered stable due to a positive hydrodynamic damping ratio: 0.07 computed by the time domain solution method and 0.06 by the frequency domain solution method, with dominant stabilising effects on the pressure side and mixed stabilising/destabilising effects on the suction side of the blade. The flow visualisation showed that the flow field and structures around the blade were distorted by the oscillatory motion of the blade, which, however, requires further investigations considering different frequencies and amplitudes of the blade structural oscillation. Extensive validations of the frequency domain solution method against the traditional time domain solution method revealed that the frequency domain method can accurately predict the hydroelastic performances of the marine current turbine blade while significantly reducing the computational cost to approximately 2.5 hours from 60 hours.

The impact of this study on industrial applications is significant. Hydroelastic analysis becomes increasingly important as lighter and more flexible blades, often made from composite materials, are developed for marine current turbines. While these materials offer advantages such as reduced weight, improved durability, and lower maintenance, the structural responses of the blade subject to the incoming hydrodynamic loads should be taken into account. However, computation time remains a significant challenge for unsteady hydroelastic simulations. The frequency domain method effectively addresses this issue by reducing computational costs and resources, making it feasible for industrial applications and concurrent design optimisations.

Acknowledgements

The authors would like to acknowledge that this research is funded by the Vice Chancellor's Early Career Research (VCECR) Award by the University of the West of England under the grant number of VCECR24-15.

Author contributions

Shine Win Naung (Conceptualization [equal], Formal analysis [equal], Funding acquisition [equal], Investigation [equal], Methodology [equal], Software [equal], Validation [equal], Writing—original draft [equal]), Yufeng Yao (Funding acquisition [equal], Visualization [equal], Writing—review & editing [equal]), Ceri Morris (Resources [equal], Writing—original draft [equal]), Allan Mason-Jones (Resources [equal], Writing—original draft [equal]), and Amir Keshmiri (Writing—review & editing [equal])

Conflict of interest

None declared.

Funding

The project was funded by the University of the West of England under the grant number of VCECR24-15.

References

1. Khojasteh D, Shamsipour A, Huang L. *et al.* A large-scale review of wave and tidal energy research over the last 20 years. *Ocean Eng* 2023;**282**:114995. https://doi.org/10.1016/j.oceaneng.2023.114995.

2. Ciaran Frost. Cost reduction pathway of tidal stream-energy in the UK and France. In: *Tidal Stream Industry Energiser. Offshore Renewable Energy Catapult*, 2022. https://cms.ore.catapult.org.uk/wp-content/uploads/2022/10/Tidal-stream-cost-reduction-report-T3.4.1-v1.0-for-ICOE.pdf.
3. Nachtane M, Tarfaoui M, Goda I. *et al.* A review on the technologies, design considerations and numerical models of tidal current turbines. *Renew Energy* 2020;**157**:1274–88. https://doi.org/10.1016/j.renene.2020.04.155.
4. Masters I, Chapman JC, Willis MR. *et al.* A robust blade element momentum theory model for tidal stream turbines including tip and hub loss corrections. *J Mar Eng Technol* 2011;**10**:25–35. https://doi.org/10.1080/20464177.2011.11020241.
5. Epps BP, Roesler BT, Medvitz RB. *et al.* A viscous vortex lattice method for analysis of cross-flow propellers and turbines. *Renew Energy* 2019;**143**:1035–52. https://doi.org/10.1016/j.renene.2019.05.053.
6. Apsley DD, Stallard T, Stansby PK. Actuator-line CFD modelling of tidal-stream turbines in arrays. *J Ocean Eng Mar Energy* 2018;**4**:259–71. https://doi.org/10.1007/s40722-018-0120-3.
7. Liu C, Hu C. An actuator line—immersed boundary method for simulation of multiple tidal turbines. *Renew Energy* 2019;**136**:473–90. https://doi.org/10.1016/j.renene.2019.01.019.
8. Ebdon T, Allmark MJ, O'Doherty DM. *et al.* The impact of turbulence and turbine operating condition on the wakes of tidal turbines. *Renew Energy* 2021;**165**:96–116. https://doi.org/10.1016/j.renene.2020.11.065.
9. Abuan BE, Howell RJ. The performance and hydrodynamics in unsteady flow of a horizontal axis tidal turbine. *Renew Energy* 2019;**133**:1338–51. https://doi.org/10.1016/j.renene.2018.09.045.
10. Wang L, Quant R, Kolios A. Fluid structure interaction modelling of horizontal-axis wind turbine blades based on CFD and FEA. *J Wind Eng Ind Aerodyn* 2016;**158**:11–25. https://doi.org/10.1016/j.jweia.2016.09.006.
11. Jiao J, Huang S, Wang S. *et al.* A CFD–FEA two-way coupling method for predicting ship wave loads and hydroelastic responses. *Appl Ocean Res* 2021;**117**:102919. https://doi.org/10.1016/j.apor.2021.102919.
12. Yang P, Xiang J, Fang F. *et al.* A fidelity fluid-structure interaction model for vertical axis tidal turbines in turbulence flows. *Appl Energy* 2019;**236**:465–77. https://doi.org/10.1016/j.apenergy.2018.11.070.
13. Win Naung S, Nakhchi ME, Rahmati M. Numerical analysis of the performance of a composite marine propeller blade subject to structural blade oscillations. *Ocean Eng* 2023;**290**:116324. https://doi.org/10.1016/j.oceaneng.2023.116324.
14. Hall KC, Thomas JP, Clark WS. Computation of unsteady nonlinear flows in cascades using a harmonic balance technique. *AIAA J* 2002;**40**:879–86. https://doi.org/10.2514/2.1754.
15. He L. Harmonic solution of unsteady flow around blades with separation. *AIAA J* 2008;**46**:1299–307. https://doi.org/10.2514/1.28656.
16. Rahmati MT, He L, Wang DX. *et al.* Nonlinear time and frequency domain methods for multirow aeromechanical analysis. *J Turbomach* 2014;**136**:041010. https://doi.org/10.1115/1.4024899.
17. Rahmati MT, He L, Li YS. The blade profile orientations effects on the aeromechanics of multirow turbomachines. *J Eng Gas Turbine Power* 2016;**138**:062606. https://doi.org/10.1115/1.4030569.
18. Win Naung S, Rahmati M, Farokhi H. Nonlinear frequency domain solution method for aerodynamic and aeromechanical analysis of wind turbines. *Renew Energy* 2021;**167**:66–81. https://doi.org/10.1016/j.renene.2020.11.046.
19. Win, Naung S, Rahmati M, Farokhi H. Aeromechanical analysis of a complete wind turbine using nonlinear frequency domain solution method. *J Eng Gas Turbine Power* 2021;**143**:011018. https://doi.org/10.1115/1.4049206.
20. Win Naung S, Nakhchi ME, Rahmati M. High-fidelity CFD simulations of two wind turbines in arrays using nonlinear frequency domain solution method. *Renew Energy* 2021;**174**:984–1005. https://doi.org/10.1016/j.renene.2021.04.067.
21. Morris C, Mason-Jones A, O'Doherty DM. *et al.* The influence of solidity on the performance characteristics of a tidal stream turbine. In: *European Wave and Tidal Energy Conference, Nantes, France, 6–11 September 2015*. Cardiff University. https://orca.cardiff.ac.uk/id/eprint/81362.
22. Morris CE, O'Doherty DM, Mason-Jones A. *et al.* Evaluation of the swirl characteristics of a tidal stream turbine wake. *Int J Mar Energy* 2016;**14**:198–214. https://doi.org/10.1016/j.ijome.2015.08.001.
23. Mason-Jones A, O'Doherty DM, Morris CE. *et al.* Non-dimensional scaling of tidal stream turbines. *Energy* 2012;**44**:820–9. https://doi.org/10.1016/j.energy.2012.05.010.
24. Patil S, Zori L, Galpin P. *et al.* Investigation of time/frequency domain CFD methods to predict turbomachinery blade aerodynamic damping. *Proceedings of ASME Turbo Expo 2016: Turbomachinery Technical Conference and Exposition, Seoul, South Korea. 13-17 June 2016*. https://doi.org/10.1115/GT2016-57962.
25. Win Naung S, Nakhchi ME, Rahmati M. Prediction of flutter effects on transient flow structure and aeroelasticity of low-pressure turbine cascade using direct numerical simulations. *Aerosp Sci Technol* 2021;**119**:107151. https://doi.org/10.1016/j.ast.2021.107151.

International Journal of Low-Carbon Technologies, 2025, 20, 1627–1637
https://doi.org/10.1093/ijlct/ctaf094
Original Article